



CHARACTERISTICS OF SiO₂/TiO₂ NANOCOMPOSITE PARTICLES FORMED IN A PREMIXED FLAT FLAME

S. H. Ehrman,*† S. K. Friedlander*§ and M. R. Zachariah‡

* Aerosol Technology/Air Quality Laboratory, Department of Chemical Engineering, 5531 Boelter Hall, University of California, Los Angeles, CA 90095, U.S.A.

‡ Chemical Science and Technology Laboratory, Building 221 Room B312, National Institute of Standards and Technology Gaithersburg, MD 20899, U.S.A.

(First received 10 April 1997; and in Final form 8 August 1997)

Abstract—Nanometer sized ($d_p = 15$ nm) SiO₂/TiO₂ particles were generated in a premixed flat flame aerosol reactor from three sets of precursors: SiBr₄/TiCl₄, SiCl₄/TiCl₄, and hexamethyl disiloxane (HMDS)/TiCl₄. Single component silica and titania aerosols were also generated from SiBr₄, SiCl₄, HMDS and TiCl₄. The choice of silica precursor had no observable effect on the particle size of the single component aerosols, or on the distribution of species in the mixed aerosol, as determined by transmission electron microscopy (TEM) and by interparticle chemical analysis of the mixed aerosol using energy dispersive X-ray spectrometry (EDS). These results suggest that for this flame configuration, chemical processes are not rate determining for particle size and do not affect the arrangement of species for mixed systems. Within the particles, small (3–12 nm in diameter) crystalline regions enriched in titanium were observed using electron energy loss spectrometry (EELS) coupled with scanning transmission electron microscopy (STEM). A mechanism in which segregation occurs during particle growth by diffusion *within* the particles is proposed.

© 1998 Elsevier Science Ltd. All rights reserved

NOMENCLATURE

a	surface area of coalescing particles, cm ²
a_s	surface area of spherical equivalent, cm ²
d_p	particle diameter, cm
d_s	seed particle diameter, cm
D	solid state diffusion coefficient, cm ² s ⁻¹
E_a	activation energy for precursor decomposition, kJ mol ⁻¹
k	Boltzmann constant, 1.3807 × 10 ⁻¹⁶ g cm ² s ⁻² K ⁻¹
k_0	preexponential for precursor decomposition, s ⁻¹
m	number of particles coalescing together
N_0	initial number concentration of precursor molecules, cm ⁻³
N_s	number concentration of seed particles, cm ⁻³
P_a	ambient pressure, atm
P_i	interior pressure, atm
r	particle radius, cm
R	monomer production rate, cm ⁻³ s ⁻¹
R_{\max}	maximum allowable monomer production rate, cm ⁻³ s ⁻¹
t	time, s
$t_{95 \min}$	minimum time allowed for 95% of precursor to react, s
$t_{95 r \times n}$	time for 95% of precursor to react based upon decomposition kinetics, s
T	temperature of the gas,
T_0	reference temperature, K
U_0	reference velocity at the reference temperature, cm s ⁻¹
v_m	molecular volume, cm ³
v_0	molecular volume for diffusion, cm ³
v_p	particle volume, cm ³
V	aerosol volume loading, cm ³ aerosol cm ⁻³ gas
x	distance from the flame along centerline, cm
<i>Greek letters</i>	
η	viscosity, Pa s
σ	surface tension, J m ⁻²
τ_c	characteristic coalescence time, s

† Present address: Laboratory for Radio and Environmental Chemistry, Paul Scherrer Institute, CM-5232 Villigen, PSI, Switzerland.

§ Author to whom correspondence should be addressed.

INTRODUCTION

The use of aerosol flame reactors to produce materials such as carbon black, fumed silica, and titania is well established on an industrial scale (Ulrich, 1984). Flame processing can be used to produce materials of high purity, without the multiple steps and high liquid volumes associated with wet chemical processes (Pratsinis and Mastrangelo, 1989).

Many studies of the formation of single species oxide aerosol by gas-to-particle conversion in flame reactors have been conducted for example by Formenti *et al.* (1972), Ulrich (1971), Chung and Katz (1985), Zachariah (1990) and Windeler *et al.* (1997a, b). In contrast, there have been relatively few studies of the formation of mixed oxide aerosol in flames (Hung and Katz, 1992; Hung *et al.*, 1992; Miquel *et al.*, 1993; Vemury and Pratsinis, 1995; Zachariah *et al.*, 1995a, b). In this work, both single component silica and titania aerosol, and mixed $\text{SiO}_2/\text{TiO}_2$ aerosol were generated in a premixed methane flat flame reactor. The observed primary particle sizes of the single component aerosol were compared with predictions of primary particle size made using the collision/sintering theory of Koch and Friedlander (1990). The predictions were made using both experimentally obtained sintering parameters, and parameters derived from literature values for the solid state diffusion coefficient of titania and the viscosity of silica.

In the mixed aerosol portion of this study, a method was developed for characterizing the degree of mixing in a binary aerosol system, $\text{SiO}_2/\text{TiO}_2$, using analytical electron microscopy techniques. Both the intraparticle and interparticle distribution of chemical species were examined. The distribution of species from particle to particle was determined using energy dispersive X-ray spectroscopy (EDS) coupled with transmission electron microscopy (TEM). This procedure was used to investigate the effect of silica precursor choice on the distribution of species in the mixed aerosol. Electron energy loss spectrometry (EELS) coupled with scanning transmission electron microscopy (STEM) was used to determine the distribution of species within the particles.

The observed results can be explained by considering the probable mechanism of precursor decomposition in a premixed flame environment, and the equilibrium phase distribution of the $\text{SiO}_2/\text{TiO}_2$ system at the temperatures encountered in the flame. A simple criteria, developed for runaway nucleation in single component systems by Zachariah and Dimitriou (1990), was applied to the general case of binary particle formation to determine conditions for which the formation of either chemically uniform or chemically distinct particles is likely.

The mixed system, $\text{SiO}_2/\text{TiO}_2$, was chosen for study because of its interesting material properties, and because of the important industrial applications of mixed $\text{SiO}_2/\text{TiO}_2$ materials, some of which are listed in Table 1. Silica is a strong network former, and is amorphous as formed in flame reactors (Ulrich, 1971). Flame processed titania, in contrast, is crystalline (Solomon and Hawthorne, 1991). In the solid phase, there is no thermodynamically stable mixed phase, although experimentally, solubility of titania in silica glasses has been observed up to mass fraction of 12% of titania (Schultz, 1976). In the liquid phase, for compositions ranging from approximately mass fraction of 20–90% titania, the liquids are immiscible (DeVries *et al.*, 1954). The desired distribution of species depends on the application. For example, for low thermal expansion glasses containing less than 12% by weight titania in silica, complete mixing is desired (Schultz, 1976). However, in optical waveguide cladding applications, phase separated regions enriched in titania improve the fatigue resistance of the optical fiber by preventing the spread of cracks (Backer *et al.*, 1991).

The effect of microstructure on the properties of multicomponent materials has been the subject of extensive study. However, the effects of processes occurring during aerosol formation on the microstructure of the resulting aerosol materials have not been addressed. The goal of this study is to relate the observed distribution of species in the mixed aerosol to the process conditions and the equilibrium behavior of system.

Table 1. Industrial applications of SiO₂/TiO₂ materials

Application	Composition	Morphology	Reference
Low thermal expansion glass	up to 8 wt % TiO ₂	Homogenous solution of TiO ₂ in SiO ₂	Gregor <i>et al.</i> (1983)
Fatigue resistant optical fiber cladding	10.5 wt % TiO ₂ upto 13 wt % TiO ₂	Crystals of anatase TiO ₂ in SiO ₂ /TiO ₂ mixture	Backer <i>et al.</i> (1991)
Catalysts and catalyst supports	7 to 97 wt % TiO ₂ in SiO ₂	Homogenous or TiO ₂ on surface of SiO ₂	Ko <i>et al.</i> (1987) Sohn and Jang (1991) Kumphar (1993) Liu and Davis (1994)
Chalk resistant paint pigments (SiO ₂ usually in combination with Al ₂ O ₃)	3–5 wt % to 10 wt % of pigment particle	Coating of SiO ₂ /Al ₂ O ₃ on surface of particle	Solomon and Hawthorne (1991)

EXPERIMENTAL

A schematic of the experimental apparatus for generation of SiO₂/TiO₂ aerosols from gas-phase precursors is shown in Fig. 1.

Precursor delivery

Titanium (IV) chloride (TiCl₄, 99.9%, Cerac Inc.) was used as the precursor for titania. Silicon (IV) bromide (SiBr₄, 99 + %, Strem Chemicals), silicon (IV) chloride (SiCl₄, 99.999%, Aldrich Inc.), and hexamethyl disiloxane (HMDS, 98 + %, Aldrich Inc.) were used as the silica precursors. Certain commercial products and instruments are identified to adequately specify the experimental procedure. In no case does such identification imply endorsement by the National Institute of Standards and Technology. These compounds are liquids with significant vapor pressures (greater than 900 Pa) at room temperature, and were delivered to the flame by bubbling dried filtered nitrogen through the liquids. To measure the precursor delivery rate to the flame, gravimetric determinations were made

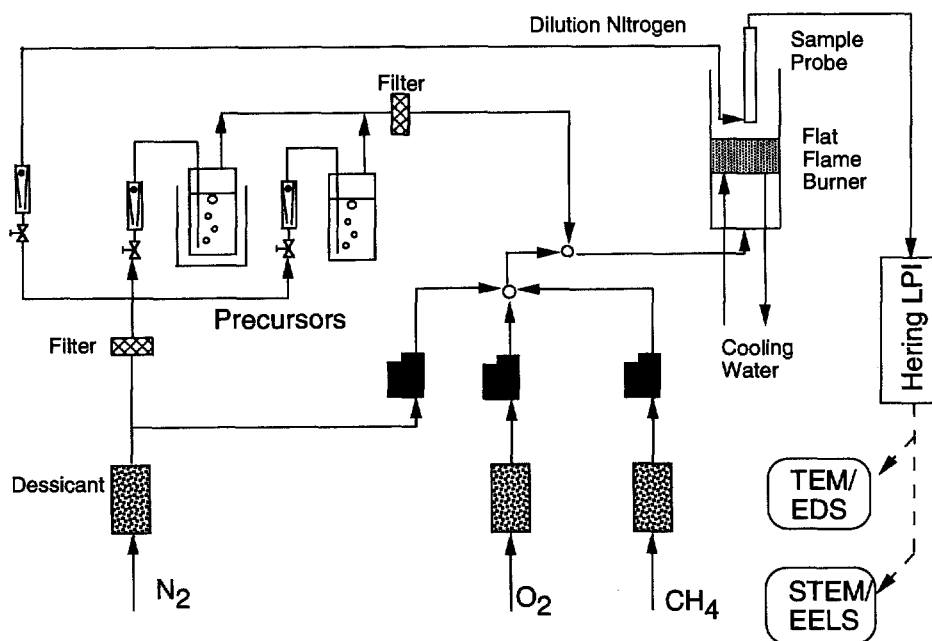


Fig. 1. Apparatus for generation of binary aerosols from gas-phase precursors.

using a condensation trap of the nitrogen stream as a function of nitrogen flow rate through the bubbler (Ehrman, 1997). To remove particles formed by bubble bursting, a 25 mm diameter Gelman type A/E glass fiber filter was installed downstream of the bubblers. Because SiCl_4 is significantly more volatile than TiCl_4 , SiBr_4 , or HMDS, the SiCl_4 bubbler was kept in an ice water bath. The flow rates of the precursors were chosen to correspond to a 1:1 mole ratio of Si to Ti in the flame, so as to maintain a mole concentration of each precursor in the flame of $8.7 \times 10^{-6} \text{ mol l}^{-1}$ ($4.4 \times 10^{-6} \text{ mol l}^{-1}$ of HMDS) at standard temperature and pressure. Experiments were also conducted for the single component case for each precursor at the same mole concentrations.

Flat flame burner

The flame configuration chosen was a laminar premixed $\text{CH}_4/\text{N}_2/\text{O}_2$ flat flame reactor. It has the advantage of a simple geometry, and also serves as a model of more complicated industrial processes such as the Cab-O-Sil process, which is also based on premixed hydrocarbon flame methods (Ulrich, 1971). The burner consists of a gravity sintered bronze plug, 4.5 cm thick and 5 cm in diameter, void fraction approximately 0.5. The plug is encased in a stainless steel sleeve, and sealed with o-rings, as shown in Fig. 2. A radially uniform flame was stabilized approximately 1.5 mm above the surface of the burner. To prevent sintering of the burner surface, a cooling coil circulating chilled house water was built into the plug during the gravity sintering step, positioned parallel to and one centimeter below the surface.

The flow rates of the gases (methane, 99.99%; oxygen 99.98%; nitrogen, 99.5%; MG Industries) are given in Table 2. The flows of the flame gases were controlled using mass flow controllers (model FC 261, Tylan Co.). The flow rates of dilution nitrogen and of nitrogen through the precursor bubblers were controlled with rotameters. The flame conditions corresponded to excess oxygen, to promote complete oxidation of the precursors. The temperature profile was measured in the absence of precursor species along the centerline with a type S (platinum-platinum/10% rhodium) fine wire thermocouple, coated with silica to minimize radical recombination reactions on the wire surface, and corrected for radiation losses (Bradley and Matthews, 1968). The corrected profile is shown in Fig. 3. A least-squares fit of the temperature profile gives a cooling rate of approximately 106 K cm^{-1} for the first five centimeters, and 60 K cm^{-1} further downstream. The computed adiabatic flame temperature is 1857 K. The difference between the adiabatic flame

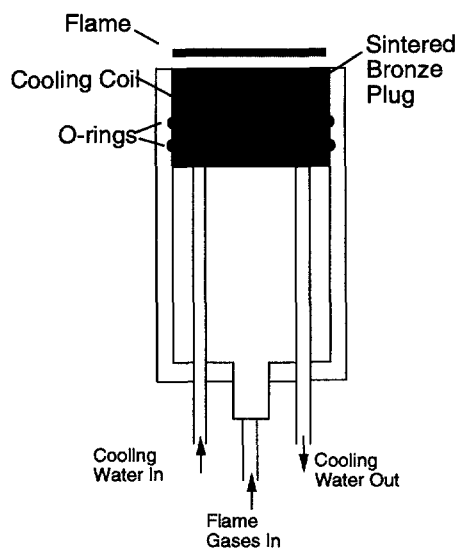


Fig. 2. Detail of premixed $\text{CH}_4/\text{N}_2/\text{O}_2$ flat flame reactor.

Table 2. Reactant flow rates for synthesis of silica, titania and SiO₂/TiO₂ composite particles

Flow rates, l m ⁻¹ at STP	SiBr ₄ /TiCl ₄	SiCl ₄ /TiCl ₄	HMDS/ TiCl ₄	SiBr ₄ only	SiCl ₄ only	HMDS	TiCl ₄
Methane	1.0	1.0	1.0	1.0	1.0	1.0	1.0
Flame nitrogen	8.9	9.4	9.3	9.2	9.6	9.6	9.4
Oxygen	3.2	3.2	3.2	3.2	3.2	3.2	3.2
Nitrogen to Si precursor*	0.45 (0.28)	0.026 (0.026)	0.038 (0.030)	0.45 (0.28)	0.026 (0.026)	0.038 (0.030)	
Nitrogen to Ti precursor*	0.22 (0.17)	0.22 (0.17)	0.22 (0.17)				0.22 (0.17)

* Parentheses indicate flow rate assuming nitrogen leaving the precursor bubblers is saturated with precursor vapor.

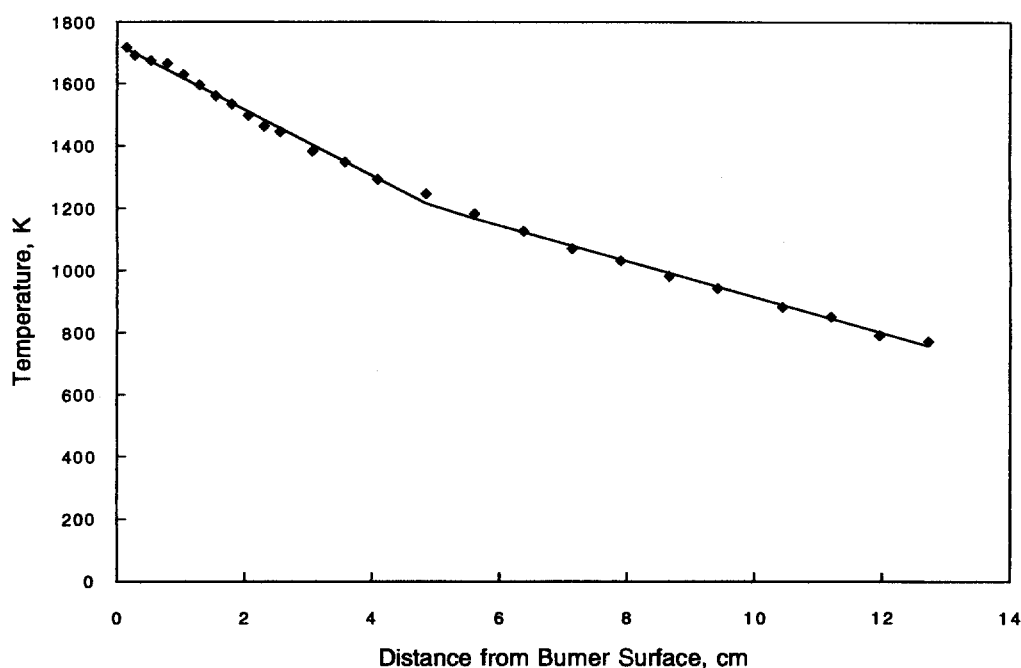


Fig. 3. Temperature profile along centerline of flame, measured with a type S thermocouple and corrected for radiation losses. The maximum measured flame temperature was 1720 K.

temperature and the maximum measured flame temperature (1720 K) can be attributed to heat losses to the burner plug, while the decrease in temperature downstream can be attributed to radiative and convective losses to the glass flame shroud.

Because of the reactivity of the halide precursors with water, all gases were passed through desiccant canisters containing anhydrous calcium sulfate (Drierite). In addition, to minimize adsorption of water on the surface of the porous burner plug, and subsequent desorption, the burner plug and housing were stored in an oven maintained at 150°C between experiments.

Sampling for TEM

The aerosol was sampled for TEM with a nitrogen aspirated sampling probe at a height of four centimeters above the flame, corresponding to a residence time of approximately 6 hundredths of a second. Dried, filtered nitrogen was supplied to the tip of the probe in a ten to one volume ratio of dilution gas to sampled air. Dilution served to quench coagulation, and to prevent water from condensing on the particles. The critical orifice and stage 6 of the Hering Low Pressure Impactor (Hering *et al.*, 1979) were used to deposit the

particles onto TEM grids (copper, 200 mesh, Type B formvar, Ted Pella Inc.). Determination of the Stokes number for the sampling conditions indicated that particle inertia is negligible for particles less than one micron, and therefore, isokinetic sampling was not necessary to ensure representative sampling with respect to particle size (Hinds, 1982).

Microscopy and chemical analysis

A Phillips EM400 TEM equipped with a NORAN Explorer X-ray detector was used to image the particles and for qualitative chemical analysis of individual particles using energy dispersive X-ray spectrometry (EDS). The purpose of this analysis was to determine if the individual particles contained both silicon and titanium. The microscope was calibrated using a thin film standard reference material of known thickness and composition (NIST SRM 2063a) under the same operating conditions used during the analysis of the aerosol samples (Ehrman, 1997). The electron beam diameter ranged from 20–30 nm. Because of the random motion of electrons in the sample, the actual analyzed area is larger than the probe diameter (Hren *et al.*, 1979). To ensure that single particle analysis was taking place, spectra were taken only from isolated particles on the grid.

To determine the distribution of species within the particle, the particles were analyzed using a VG Microscopes HB501 scanning transmission electron microscope (Fisons Instruments) equipped with a Gatan model 666 electron energy loss spectrometer (Gatan Inc.). The electron beam probe size ranged from 1–3 nm in diameter. Resolution approximately equal to the probe diameter is achieved with EELS because electrons which are scattered out of the probe volume and therefore interacting with material outside of the probe volume are not detected (Eberhart, 1991).

RESULTS

Single component aerosols

Single component silica aerosol was produced using SiBr_4 , SiCl_4 and HMDS as precursors. Titania was generated from TiCl_4 . TEM images of the single component particles are shown in Fig. 4. The primary particle size was determined from the TEM images by measuring the diameter of 50 particles in a sample and averaging the measurements. In the case where the particles were not roughly spherical, the average of the smallest and largest dimensions was taken to be the diameter. The average primary particle size was approximately 10 ± 1 nm for each silica sample. The similarity in particle size in the silica samples suggests that there are no significant differences in the chemical reaction behavior of the precursors in the flame. All of the silica samples are amorphous.

The pure titania aerosol is crystalline and faceted. The crystal structure of the titania aerosol as determined by selected area electron diffraction is anatase. The average particle size is slightly larger for titania ($d_p = 13 \pm 1$ nm) than for silica formed under the same conditions. This may be because of differences in coalescence behavior between silica and titania. Titania coalesces by solid state diffusion at a rate much greater than the viscous flow coalescence of silica (Xiong *et al.*, 1993). This result has been observed for the case of silica and titania formation in a tube furnace reactor by Xiong *et al.* (1993) although the difference in particle size was much greater in the furnace reactor studies ($d_p = 60$ nm for titania compared to $d_p = 7$ nm for silica). The reason for the large particle size difference in the furnace reactor may be the longer residence time for the furnace, on the order of a second, versus a residence time of hundredths of a second in the flame.

Single component: comparison of particle size with estimates using collision/sintering theory

For the growth of primary particles by coalescence, the final primary particle size for single component systems can be estimated using the collision/sintering theory of Koch and

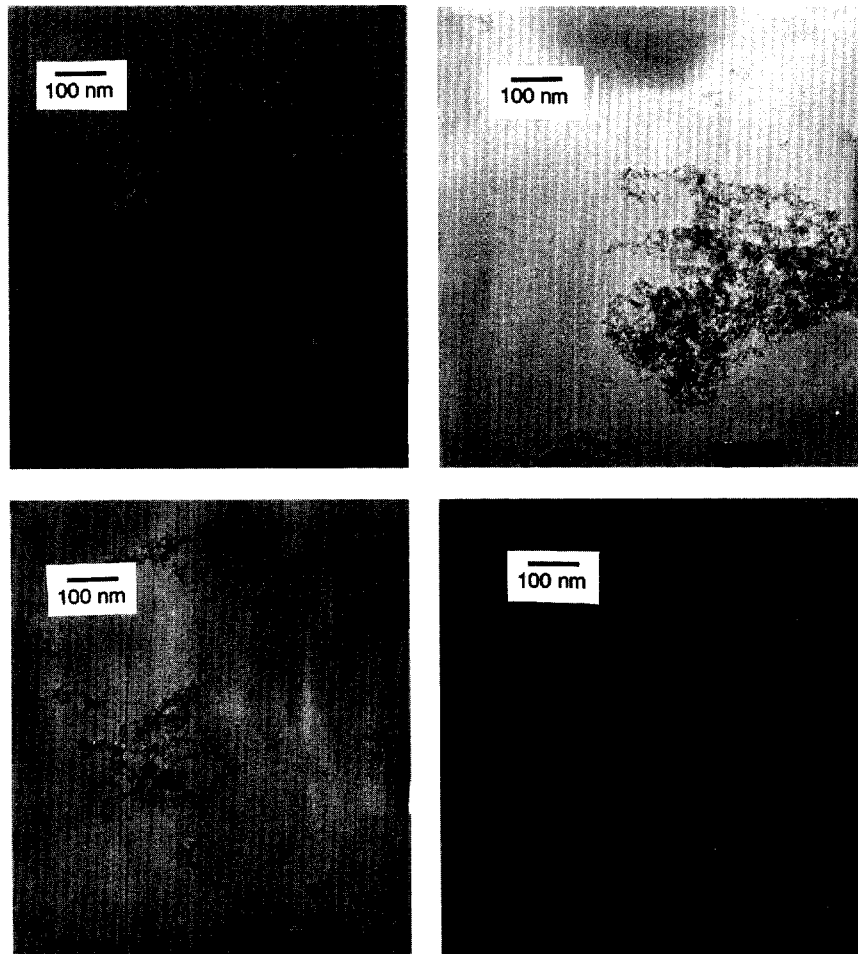


Fig. 4. Single component aerosol. (a) Titania from TiCl_4 , average primary particle diameter = 13 nm. (b) Silica from SiBr_4 , average primary particle diameter = 10 nm. (c) Silica from SiCl_4 , average primary particle diameter = 10 nm. (d) Silica from HMDS, average primary particle diameter = 10 nm.

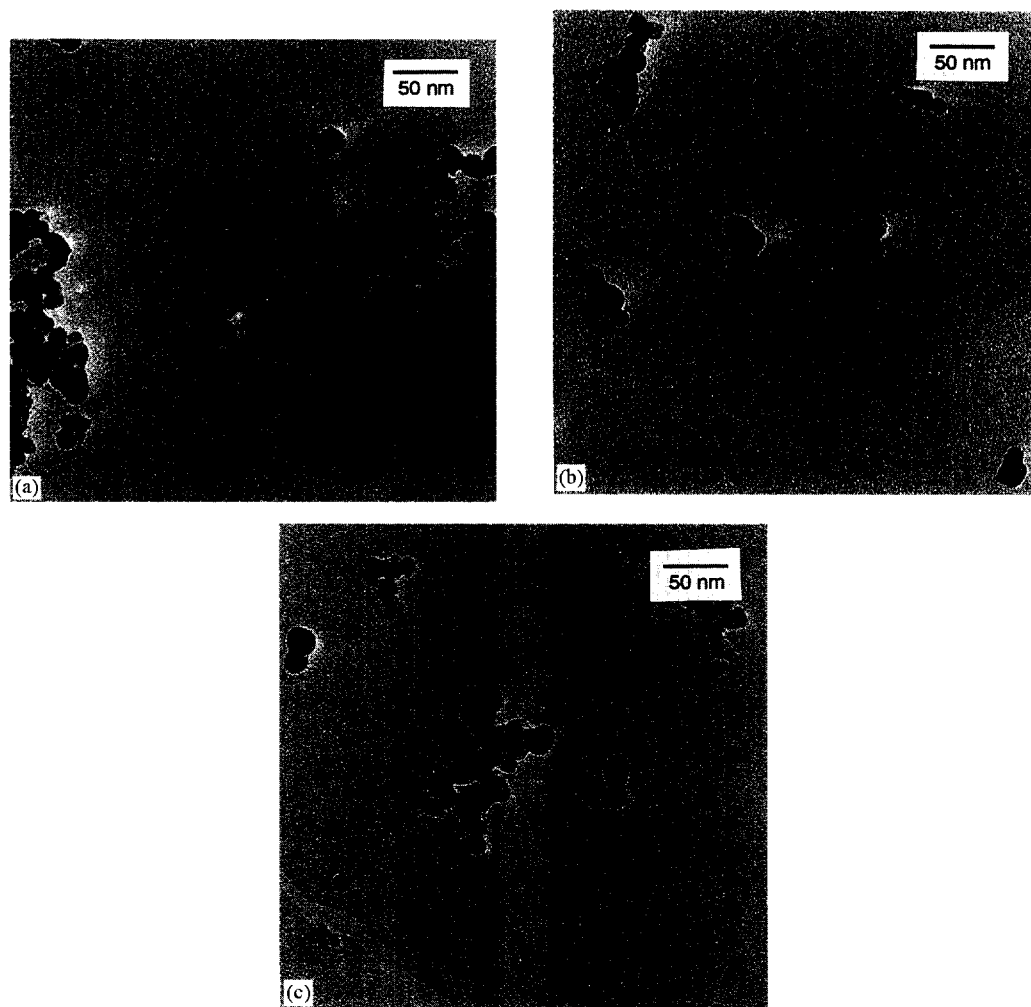


Fig. 5. $\text{SiO}_2/\text{TiO}_2$ aerosol from (a) $\text{SiBr}_4/\text{TiCl}_4$, (b) $\text{SiCl}_4/\text{TiCl}_4$, and (c) $\text{HMDS}/\text{TiCl}_4$. The average particle diameter for each sample was approximately the same, 15 nm.

Friedlander (1990):

$$da/dt = -(1/\tau_f)(a - a_s) \quad (1)$$

where a is the surface area of the coalescing particles, a_s is the surface area of a single spherical particle of the same volume, and τ_f is the characteristic coalescence time.

For sintering by solid state diffusion, as in the case of titania, the characteristic coalescence time is represented by an equation of the form

$$\tau_f = 3kTv_p/64\pi D\sigma v_0. \quad (2)$$

Here, σ is the surface tension, v_0 is the molecular volume for diffusion, v_p is the particle volume, and D is the solid state diffusion coefficient, usually reported as an Arrhenius function of temperature in the literature (Friedlander and Wu, 1994). For silica, which is assumed to sinter by a viscous flow mechanism, the characteristic coalescence time is given by

$$\tau_f = \eta d_p/\sigma \quad (3)$$

where d_p is particle diameter and η is viscosity, which for silica displays Arrhenius-like behavior as a function of temperature (Frenkel, 1945).

In the manner of Lehtinen *et al.* (1996), the variables are changed from particle surface area to particle volume,

$$dv_p/dt = (3v_p/\tau_f)(m^{-1} - m^{-4/3}). \quad (4)$$

Here, m is the number of particles which are coalescing together, taken to be two in this simple analysis. The temperature is assumed to be radially uniform, decreasing linearly with distance from the flame, with a cooling rate of approximately 106 K cm⁻¹. Assuming plug flow, the distance from the flame can be related to the residence time,

$$dx/dt = (U_0/T_0) T(x) \quad (5)$$

where U_0 is the reference velocity at the reference temperature T_0 and $T(x)$ is the temperature profile.

Equations (4) and (5) were solved numerically for the formation of silica and titania in the flame using two sets of characteristic coalescence times, given in Table 3. The first two characteristic coalescence times were derived from equations (2) and (3) for titania and silica respectively, by substituting bulk property data given in Table 4. The second two were obtained experimentally by Xiong *et al.* (1993). A two-dimensional discrete-sectional aerosol growth model was fit to experimental particle size data for the formation of silica and titania in a tube furnace using characteristic coalescence time as the adjustable parameter.

The model results are shown in Table 5. An estimate of particle size calculated using the coalescence time derived from bulk property data compared well with the observed primary particle size for titania, but primary particle size was overestimated when the coalescence time from a fit to experimental data was used. In this and in other work (Windeler *et al.*, 1997b) where primary particle size predictions were made using characteristic coalescence times derived from solid state diffusion data, relatively good agreement was seen between observed and predicted particle size.

The primary particle size for silica was underpredicted when either characteristic coalescence time was used. In both cases, the growth rate was so slow that the particle size did not increase significantly beyond the size of a silica monomer. The poor agreement between experimental primary particle size and model predictions suggests that either the viscosity of the silica nanoparticles is considerably lower than that of the bulk material or that sintering takes place by a mechanism other than viscous flow. It is known that the presence of trace amounts of impurities such as alkali metals and hydroxyl groups in silica can significantly lower viscosity (Scholze, 1990). Incorporation of hydroxyl groups occurs as

Table 3. Characteristic coalescence times used in calculations of particle size

Species	Characteristic coalescence time	Reference
Silica, property data	$\tau_r = 6.3 \times 10^{-10} d_p \exp(6.1 \times 10^4/T)$	Calculated from data in Table 3
Titania, property data	$\tau_r = 1.5 \times 10^3 T d_p^3 \exp(3.4 \times 10^4/T)$	Calculated from data in Table 3
Silica, model fit	$\tau_r = 5.5 \times 10^5 d_p \exp(1565/T)$	Xiong <i>et al.</i> (1993)
Titania, model fit	$\tau_r = 8.3 \times 10^{16} T d_p^4 \exp(3700/T)$	Xiong <i>et al.</i> (1993)

Table 4. Bulk property data used in equations (2) and (3) to calculate characteristic coalescence times

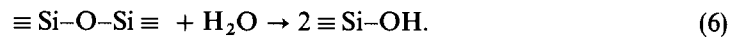
Property	Value	Reference
Silica, surface tension*, $J m^{-2}$	0.3	Parikh (1958)
Silica, viscosity, Pa s	$1.9 \times 10^{-8} \exp(6.1 \times 10^4/T)$	Hetherington <i>et al.</i> (1964)
Titania, diffusivity, $cm^2 s^{-1}$	$7.2 \times 10^{-2} \exp(-3.4 \times 10^4/T)$	Astier and Vergnon (1976)
Titania, molecular volume for diffusion, cm^3	1.6×10^{-23}	Anderson (1967)
Titania, surface tension*, $J m^{-2}$	0.5	Bruce (1965)

*Surface tension reported for an average post-flame temperature of 1500 K.

Table 5. Comparison of experimental and calculated primary particle size

	Experimental primary particle size (nm)	Calculated particle size, τ_r from property data in Table 3 (nm)	Calculated particle size, τ_r from Xiong <i>et al.</i> (1993), (nm)
Silica	10	0.4	0.4
Titania	13	14	20

water vapor dissolved in silica reacts by hydrolysis of siloxane bonds, weakening the network:



The activation energy for viscous flow of silica has been observed to decrease with increasing hydroxyl content (Hetherington *et al.*, 1964). The viscosity parameters used in the particle size estimations were determined from measurements of Spectrosil, silica powder produced by flame hydrolysis of silicon tetrachloride, with a hydroxyl mole fraction of 0.43% (Hetherington *et al.*, 1964). Though the hydroxyl content of the silica produced in this study was not measured, it is likely to be comparable since it was also produced in a flame environment. Despite this consideration, the final particle size of silica was underpredicted. However, in addition to the effect of hydroxyl groups, the rapid collision/coalescence processes occurring in the early stages of particle growth may also limit the extent to which the silica network can form. The combination of these two effects may result in lower viscosity for silica particles in the initial stages of formation, leading to faster particle growth than that predicted using bulk viscosity values.

The ability of particle formation models to predict primary particle size is limited by the accuracy of the material property values used to determine characteristic coalescence times. For example, reported values for solid state diffusivity can vary by orders of magnitude. In addition, as discussed for silica, it is questionable whether nanometer sized particles have the same material properties as their bulk counterparts. One alternative is to infer characteristic coalescence times by fitting models to experimental data, as done by Xiong *et al.* (1993). However, the robustness of these sintering parameters to other time-temperature histories is also questionable.

Effect of precursor chemical composition

Mixed SiO₂/TiO₂ aerosol were generated from three sets of precursors: SiBr₄/TiCl₄, SiCl₄/TiCl₄, HMDS/TiCl₄. In each case, the flow rate of the precursors corresponded to a 1:1 mole ratio of silica to titania. TEM images of the particles are shown in Fig. 5. The mixed aerosol consists of spherical or near-spherical particles. The average primary particle size is approximately 15 ± 1 nm for each sample. Again, the lack of a significant difference in particle size suggests that the chemical reactions generating condensable molecules are much faster than aerosol formation processes. Within each primary particle, one or two strongly diffracting regions (3–12 nm in diameter), an indication of crystallinity, are visible as dark areas in the TEM images. Because the contrast depends in part on the orientation of the crystalline region with respect to the electron beam, some regions appear very dark, while others may be barely visible (Eberhart, 1991).

For all combinations of precursors, selected area electron diffraction revealed the crystal-line structure of titania as anatase. While rutile is the thermodynamically favored phase for titania at the maximum measured flame temperature (DeVries *et al.*, 1954), it has been observed however, that the anatase phase is usually formed in high-temperature processes. The transformation to rutile requires longer residence times and/or higher temperatures (Kobata *et al.*, 1991; Akhtar *et al.*, 1991), or the addition of a dopant such as CuO or LiF to promote the transformation (MacKenzie, 1975). The rutile transformation may be inhibited by the presence of cations of the same or greater valency than Ti⁴⁺ in interstitial sites in the lattice (Shannon and Pask, 1965). Si⁴⁺ is small enough to enter the titania lattice interstitially (Shannon and Prewitt, 1969), and indeed, in tube furnace experiments, silica inhibits the anatase-to-rutile transition (Akhtar *et al.*, 1992).

The addition of silica also changed the morphology of titania particles formed in tube furnace experiments from faceted in the absence of silica, to spherical (Akhtar *et al.*, 1992). The authors suggest that the presence of Si⁴⁺ retards the sintering of titania, slowing the rearrangement to the lowest energy faceted morphology, resulting in spherical particles. We observed similar morphologies in the flame-made mixed aerosols.

To determine if silicon and titanium were both present in the individual particles, energy dispersive X-ray analysis was conducted on isolated single particles. We followed a protocol in which 24 analyses were conducted per sample. The mole percent Ti on a metals basis was estimated for each analysis. The results are shown as a scatter plot in Fig. 6. Because of the small amounts of mass analyzed and the calibration uncertainty, substantial measurement uncertainty is associated with this technique (estimated at 24% relative; Williams and Carter (1996)). The relative error is approximately the same for each of the precursor combinations, and for clarity, error bars are shown only for the SiBr₄/TiCl₄ sample. Nonetheless, the results indicate that the particles contain both species, in approximately the same concentrations as the starting materials. No particles containing just one of the species were detected, and there were no differences among the samples, suggesting that the choice of precursor had no effect on particle homogeneity.

To investigate the composition of the crystalline domains, another analytical electron microscopy technique, electron energy loss spectrometry (EELS), was used. The microscope was operated under conditions corresponding to a probe diameter of one to three nanometers. SiO₂/TiO₂ aerosol made from SiCl₄/TiCl₄ was analyzed. Because the microscope provides only a two-dimensional view of the particle, we cannot be certain the probe was positioned entirely within the region of interest. However, significant differences in composition between the crystalline domains and the rest of the particle were observed. The crystalline regions were strongly enriched in titanium (Ti/Si ratio ranged from 3 to 18) and the non-crystalline regions were enriched in silicon (Si/Ti ratio ranged from 1.4 to 3). The strong enrichment of titanium in the crystalline regions suggests that the regions precipitated out as a relatively pure phase from within the mixed particles.

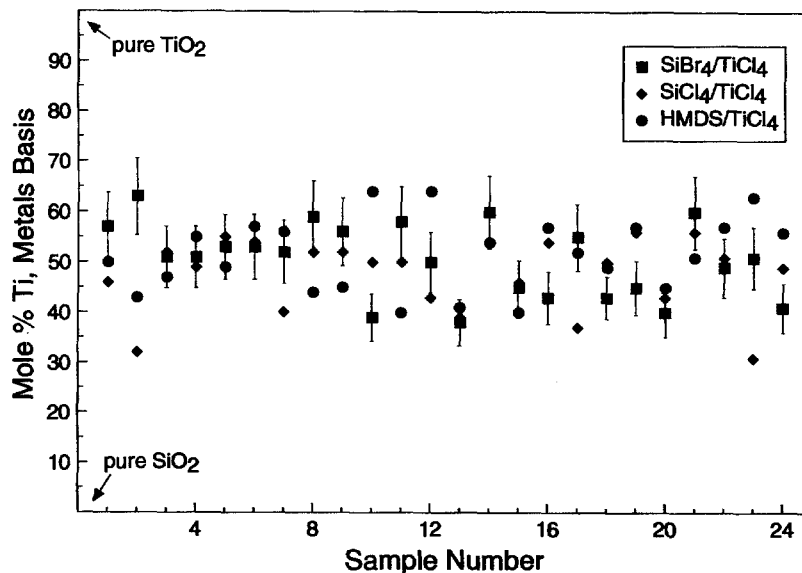


Fig. 6. Results of single particle analyses using energy dispersive X-ray spectrometry. Uncertainty bars representing an estimate of the measurement uncertainty are shown for the SiBr₄/TiCl₄ sample. The composition of the individual particles was relatively uniform with no pure particles of SiO₂ or TiO₂ detected.

DISCUSSION

Effect of precursor chemistry on particle size and the interparticle distribution of species

The processes occurring during multicomponent aerosol formation from gas-phase precursors are the same as for single component aerosol formation: chemical reaction, nucleation, and aerosol growth. The materials in this study, silica and titania, are refractory materials with low vapor pressures at the temperatures encountered in the flame. A calculation of the critical nucleus size, in the manner of Ulrich (1971) using classical nucleation theory, gives a critical nucleus size of approximately 3 Å for titania and 2 Å for silica, or less than the size of a single molecule of either titania or silica. Hence, particle formation is not governed by an activated nucleation process, since every condensable molecule can serve as a stable nucleus. Instead, particle formation is governed by kinetics of vapor-phase polymer formation, as described in Zachariah and Tsang (1993).

It is possible that differences in the chemical reaction behavior of the precursors could affect particle size for single component aerosols, and the arrangement of species for multicomponent aerosols. As an example of the effect of chemical reaction behavior on particle size, if one precursor reacted further downstream than the others, shorter residence times and smaller particles may result. This effect was observed experimentally for the formation of silica particles from silane, HMDS and tetramethyl silane (TMS) in a counter-flow diffusion burner (Zachariah and Semerjian, 1990). In these experiments, light scattering was used to observe particle growth. Silica particles from silane were detected earlier in the flame than silica particles formed from HMDS or TMS. Particle formation from TMS was observed later in the flame, and the particles were smaller, reaching a much higher number density.

The relationship between chemical reaction and the distribution of chemical species for a binary aerosol is shown for two extreme cases in Fig. 7. If the interval between the reactions is negligible compared to the time required for particle formation, then particles of uniform interparticle composition are formed, as shown in Fig. 7a. In contrast, we expect to observe chemical segregation, possibly chemically distinct primary particles, if the interval between the reactions is on the order of, or greater than the particle formation time, Fig. 7b.

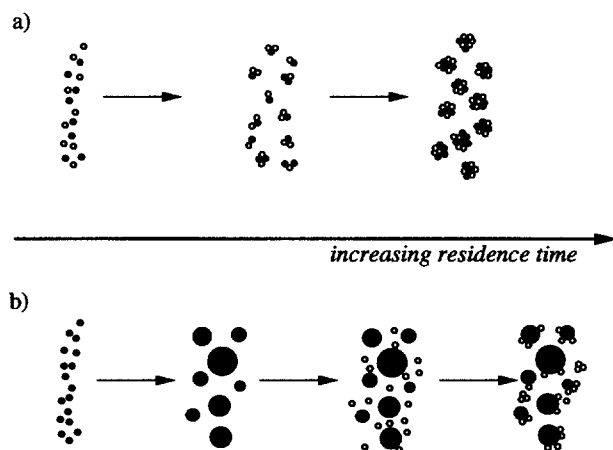


Fig. 7. Relationship between chemical reaction and the distribution of chemical species. (a) The interval between chemical reactions is negligible compared to the time required for particle formation, resulting in uniform particles. (b) The interval between chemical reactions is significant compared to the time required for particle formation, and particles varying in composition are produced.

Here, primary particles of the first species form before reaction and nucleation of the second species occurs. As the primary particles of the first species grow, the number concentration of the first species decreases by many orders of magnitude. If the chemical reaction rate of the second precursor species is sufficiently fast, then monomers of the second species will be more likely to collide with each other, at least initially. Depending on the temperature history of the process, this may result in a wider variation in chemical composition from particle to particle, and possibly formation of chemically distinct particles of the second species.

Hung and Katz (1992) observed this effect experimentally for the formation of SiO₂/TiO₂ mixed aerosol from SiCl₄/TiCl₄ in a counterflow diffusion burner. Mixed aerosol sampled at low heights in the burner, corresponding to short residence times, contained both titania particles coated with discrete silica clusters and pure silica particles. Light scattering observations of particle growth of single species silica and titania and of the mixed aerosol suggested that TiO₂ particles form before SiO₂ particles in the burner.

The counterflow diffusion burner used by Zachariah and Semerjian (1990) and Hung and Katz (1992) is characterized by a very different time-temperature history than the premixed flame configuration used in the present study. Because of the flow geometry in the counterflow diffusion burner, the precursor and particles do not pass through the reaction zone of the flame. As such, the precursor chemistry is likely governed by thermal decomposition reactions. In addition, in the precursor decomposition/particle formation region of the burner, temperature increases with increasing residence time. The species with the lowest activation energy for decomposition would be expected to react first.

In contrast, for the premixed flat flame, all gases including the precursor species pass through the reaction zone. The preheat time is on the order of a millisecond so it is unlikely that significant precursor decomposition occurs prior to the reaction zone. The reaction zone of the flame is characterized by high concentrations of radical species such as O, OH and H. As a result, the hydrocarbon combustion chemistry is dominated by low activation energy radical abstraction reactions (Glassman, 1977). One might reasonably expect the precursor compounds to behave in the same way, with the net result of fast radical driven decomposition of the precursors, with little difference between precursor reaction rates. If gas-to-particle formation follows chemical reaction, then the particles should contain both species.

Assuming that collision rate coefficients are independent of chemical composition, the relationship between chemical reactions and the distribution of species is analogous to the

problem of runaway nucleation, investigated in a numerical study by Zachariah and Dimitriou (1990). Their analysis can be applied for a binary system to compare the time scales for both radical and thermally driven precursor decomposition reactions to time scales for particle growth. The particles formed from the reaction of the first species can be considered "seed" particles. 10 nm is chosen as the characteristic diameter of particles formed from the reaction of the second species. Whether monomers of the second species will either form chemically distinct particles greater than 10 nm in diameter, or condense as monomers or sub-10-nanometer clusters onto the surface of the preexisting particles is a function of the diameter and number concentration of the preexisting particles, d_s , and N_s , respectively, and of the chemical reaction rate, R , of the second precursor species.

From numerical solutions of the Smoluchowski population balance equations, Zachariah and Dimitriou (1990) obtained an empirical correlation for the maximum allowable monomer production rate, R_{\max} , for effective scavenging as a function of seed particle diameter and number concentration:

$$R_{\max} = 1.21 \times d_s^{4.7} N_s^{2.72}. \quad (7)$$

If the monomer production rate is less than R_{\max} , monomers and sub-10-nanometer clusters will condense onto the preexisting particles, and the average particle size will increase monotonically with time. If the monomer production rate is greater than R_{\max} then chemically distinct particles (diameter 10 nm or greater) of the second species will form.

It is perhaps more physically meaningful to express this criterion in terms of the minimum allowable time for reaction of the second species. For a given volumetric loading of the second species, V , taken in this analysis to be the same as the volume loading of the first, the minimum time allowed for 95% of the precursor to react, $t_{95\min}$ is given by

$$t_{95\min} = 0.95N_0/R_{\max}. \quad (8)$$

N_0 is the initial number concentration of precursor molecules, determined from V/v_m where v_m is the molecular volume of the second species, taken to be the molecular volume of silica, $4.6 \times 10^{-23} \text{ cm}^3$. $t_{95\min}$ as a function of preexisting particle diameter for volume loadings ranging from 10^{-4} to $10^{-10} \text{ cm}^3 \text{ aerosol cm}^{-3} \text{ gas}$ is shown in Fig. 8. For comparison, the volume loadings of silica and titania in the experiments were 2.4×10^{-7} and $1.8 \times 10^{-7} \text{ cm}^3 \text{ aerosol cm}^{-3} \text{ gas}$, respectively. For a given volumetric loading, if the reaction time is less than $t_{95\min}$, monomers are generated too fast to be effectively scavenged by the preexisting particles, and formation of chemically distinct particles will occur. From Fig. 8, it is apparent that the formation of chemically distinct particles of the second species is favored for low aerosol volume loadings of large preexisting particles. Conversely, scavenging of the second species by preexisting particles of the first species is favored for high aerosol volume loadings of small preexisting particles.

These reaction times can be compared to reaction times based on estimates of the rates of chemical reactions of the precursor species. Decomposition rates have been measured for a variety of precursors in flow reactor systems. Rate parameters for SiBr_4 , SiCl_4 , HMDS and TiCl_4 , all first order with respect to precursor concentration, are presented in Table 6. Rate constants for reactions of these compounds with radical species such as hydrogen radical have not been measured. However, rates for abstraction reactions of hydrogen radicals with other halogen compounds are known. The rate parameters for the reaction of hydrogen radical with methyl chloride are also reported in Table 6 for comparison.

From the data in Table 6, the time necessary for 95% precursor reaction, $t_{95\text{rxn}}$, can be estimated for SiCl_4 , HMDS, TiCl_4 , and the hydrogen radical abstraction reaction as a function of temperature. For each species, the reaction rates were measured over a limited temperature range, given in Table 6. Here, we make the assumption that these rate parameters are valid over the entire range from 1000 to 1800 K. For the hydrogen radical abstraction reaction, a second order reaction, the concentration of hydrogen radicals in the flame is taken to be constant, estimated at $4 \times 10^{-7} \text{ mol cm}^{-3}$ (Fristrom, 1995). Because of the uncertainty in the reaction rate parameters, lower and upper bound estimates for reaction times were made assuming an activation energy of 19 kJ mol^{-1} for the lower

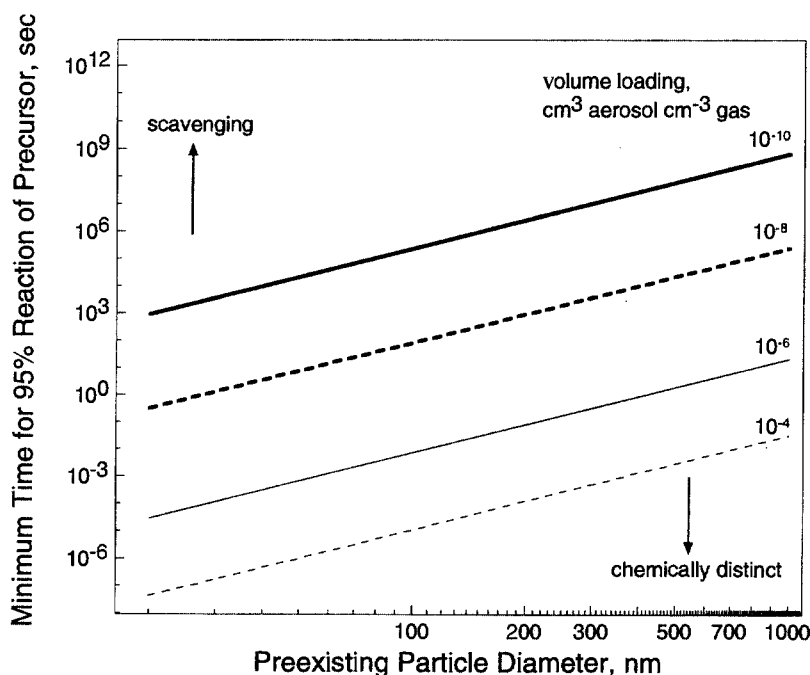


Fig. 8. Minimum time for 95% reaction of precursor for effective scavenging, $t_{95 \text{ min}}$, as a function of preexisting particle diameter and volume loading. Scavenging is favored for high volumetric loadings of small preexisting particles. Formation of chemically distinct particles of the second species is favored for low volumetric loadings of large preexisting particles.

Table 6. Rate parameters for precursor decomposition reactions

Reaction	k_0 (s ⁻¹)	E_a (kJ/mol)	Range T in (K)	Reference
$\text{SiBr}_4 + \text{O}_2 \rightarrow \text{SiO}_2 + 2\text{Br}_2$	5×10^{11}	280	1485 to 1600	French <i>et al.</i> (1978)
$\text{SiCl}_4 + \text{O}_2 \rightarrow \text{SiO}_2 + 2\text{Cl}_2$	8×10^{14}	410	1650 to 1800	French <i>et al.</i> (1978)
HMDS \rightarrow products	4×10^{17}	370	1073 to 1373	Sanogo and Zachariah (1997) and Zachariah (1997)
$\text{TiCl}_4 + \text{O}_2 \rightarrow \text{TiO}_2 + 2\text{Cl}_2$	8×10^4	89	973 to 1373	Pratsinis <i>et al.</i> (1990)
$\text{CH}_3\text{Cl} + \text{H} \cdot \rightarrow \text{CH}_3 \cdot + \text{HCl}$	4×10^{14} *	39	500 to 2500	Westenberg and DeHaas (1975)

* Because this reaction is bimolecular, the units of the preexponential are $\text{cm}^3 \text{mol}^{-1} \text{s}^{-1}$.

bound, and an activation energy of 49 kJ mol^{-1} for the upper bound estimate. The reaction times as a function of temperature are shown in Fig. 9.

Immediately apparent is the large difference between the reaction times of the halide precursors especially at temperatures less than 1600 K. For example, at 1500 K, the difference between the reaction times of the two species is on the order of tenths of seconds. The reaction of TiCl_4 is 95% complete after approximately 0.1 s, while the reaction of SiCl_4 requires approximately 1 s to reach 95% completion. Experimental observations of particle formation in premixed flames based upon *in-situ* TEM sampling as a function of residence time suggest that residence times on the order of milliseconds are sufficient for particle growth (Zachariah *et al.*, 1995a). Referring to Fig. 8, if the particles of TiO_2 reach 30 nm in diameter, then for volume loadings greater than $10^{-8} \text{ cm}^3 \text{ aerosol cm}^{-3} \text{ gas}$, the formation of chemically distinct particles of SiO_2 is favored, and for volume loadings less than $10^{-8} \text{ cm}^3 \text{ aerosol cm}^{-3} \text{ gas}$, scavenging of SiO_2 by TiO_2 is favored. From this example, it is clear that for processes in which the monomer generation rate is governed by thermal decomposition reactions such as flow reactors and counterflow diffusion burners, precursor chemistry can play an important role in determining whether scavenging or formation of chemically distinct particles will occur. It may also be possible to control the

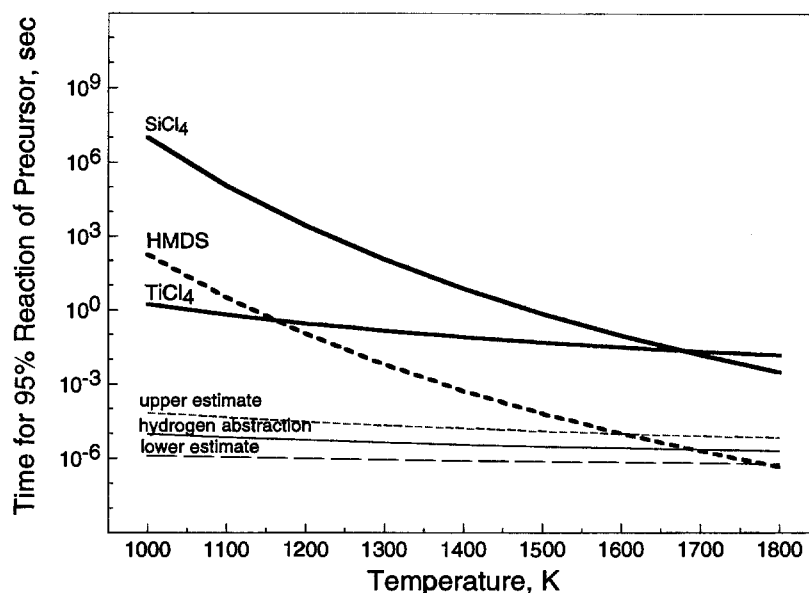


Fig. 9. Time for 95% reaction of precursor, $t_{95,rxn}$ based on measured precursor decomposition reaction rates, as a function of temperature.

arrangement of species by changing the precursors. For example at 1500 K, the reaction of TiCl_4 is complete well before the reaction of SiCl_4 . The reaction of HMDS, however, is much faster than either SiCl_4 or TiCl_4 at temperatures greater than 1200 K. If HMDS is used as the silica precursor, particles of silica would form first, leading to either titania coating silica, or discrete titania and silica particles depending on the volume loading and size to which the silica particles grow before reaction of TiCl_4 .

By comparison, reaction times based on estimated hydrogen radical abstraction rates are orders of magnitude lower than either of the halide decomposition reaction times for temperatures less than 1800 K. More importantly, the differences between the upper and lower bound estimates for reaction times are small compared to times required for particle formation. Hence, if precursor decomposition is occurring in a radical-rich flame environment, such as that found in premixed flames, the interparticle composition should be uniform, in agreement with the TEM observations reported in this study.

Intraparticle distribution of species

Though the chemical composition was relatively uniform from particle to particle (Fig. 6), chemical segregation within the particles was observed, as evidenced by the crystalline domains shown in Fig. 5 and the results of the EELS analysis. Similar results were noticed by Zachariah *et al.* (1995a) for the formation of iron oxide/silica particles in a premixed $\text{CH}_4/\text{O}_2/\text{N}_2$ Bunsen style flame. If chemical reaction behavior of the precursors is not controlling the arrangement of species in the particles, then the observed segregation within the particles must be occurring by intraparticle diffusion during particle growth as discussed by Zachariah *et al.* (1995b).

According to the phase diagram for the $\text{SiO}_2/\text{TiO}_2$ system, titania and silica are immiscible in both the liquid and solid phase at a 1:1 mole ratio. The maximum measured flame temperature is lower than the melting points of both silica and titania (1983 and 2103 K, respectively). However, it is known that the melting point of small particles decreases with decreasing particle size. Indeed, melting point depressions of as much as 25% of the bulk melting temperature have been observed for 3 nm bismuth particles (Peppiatt, 1975). As such, it is possible that the particles behave as liquids in the initial stages of growth.

We expect that in the initial stages of particle formation, conditions are closest to equilibrium because temperatures are high, particles are small and therefore, diffusional processes are rapid. At longer residence times, as the particles become larger and the temperature decreases, formation of the equilibrium phase distribution is limited by internal particle transport processes. Because of the rapid cooling in the flame reactor, we would not expect to reach the equilibrium phase distribution. We observe amorphous silica and anatase titania rather than cristobalite and rutile. However, we do observe segregation, as evidenced by the titanium-rich crystalline regions visible with TEM. Presumably, the driving force for the rearrangement is the reduction in free energy of the particles resulting from the formation of the lowest energy configuration: separate titania and silica rich phases.

Combined effect of precursor chemistry, temperature, and thermodynamics on interparticle and intraparticle mixing

Examples of possible intraparticle morphologies for various combinations of precursor decomposition behavior, temperature, and thermodynamically favored miscibility/ immiscibility are shown in Table 7. As established previously, if the precursor decomposition chemistry is radical driven, then the particles should contain both species. The arrangement within the particles, as shown in Table 7, is then a function only of the miscibility/immiscibility of the system, and of the temperature history. If the temperature is high enough that the characteristic diffusion time within the particles is on the order of the residence time, then the distribution of species will approach the thermodynamically favored arrangement. If the temperature, however, is low, achievement of the thermodynamically favored configuration will be limited by intraparticle transport. If the precursor decomposition chemistry is controlled by thermal decomposition reactions, then segregation can result either because of differences in precursor chemistry, and/or intraparticle diffusion. Again, formation of the equilibrium phase distribution is favored for high temperatures. In addition to the work by Hung and Katz (1992), examples of these effects on intraparticle homogeneity for thermally driven systems can be found in studies by Akhtar *et al.* (1992) and Akhtar *et al.* (1994) of SiO₂/TiO₂ and Al₂O₃/TiO₂ particle formation in a tube furnace reactor. In both studies, enrichment of either SiO₂ or Al₂O₃ on the surface of the particles can be attributed to differences in the precursor chemistry (Kato *et al.*, 1972; French *et al.*, 1978). Also, for the case of Al₂O₃/TiO₂ particle formation, increasing the furnace temperature from 1500 to 1700 K resulted in the formation of the thermodynamically favored mixed oxide phase, Al₂TiO₅.

The combined effect of precursor chemistry, temperature, and thermodynamics on interparticle homogeneity is shown in Table 8. If precursor decomposition is driven by radical reactions, then the individual primary particles will contain both species in

Table 7. Effect of precursor chemistry, temperature and thermodynamics on intraparticle chemical homogeneity


















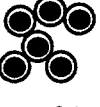


Precursor chemistry	Temperature	Miscible	Example morphology	Immiscible	Example morphology
Radical driven	High T	Uniform		Segregated	 
Radical driven	Low T	Uniform		Uniform	
Thermally driven	High T	Uniform		Segregated	 
Thermally driven	Low T	Segregated	 	Segregated	 

Table 8. Effect of precursor chemistry, temperature and thermodynamics on interparticle chemical homogeneity

Precursor chemistry	Temperature	Miscible	Example morphology	Immiscible	Example morphology
Radical driven	High T	Uniform		Uniform	
Radical driven	Low T	Uniform		Uniform	
Thermally driven	High T	Uniform		Uniform	
Thermally driven	Low T	Segregated		Segregated	

approximately the same compositions. If precursor decomposition is governed by thermal decomposition, then the temperature history of the process governs whether the interparticle composition will be uniform. If the temperature is low and/or the residence time is short, then chemically distinct particles may form as a result of differences in precursor chemistry. If the temperature is high and the residence time for particle formation is long compared to the time difference between the reactions of the precursors, then the interparticle composition could be uniform even if significant differences in precursor chemistry exist.

Lack of material property data, particularly diffusion data for multicomponent systems, makes it difficult to analyze these systems quantitatively. An additional uncertainty in our understanding of nanometer-sized particles arises from the pressure within the particles themselves. This interior pressure may affect the equilibrium phase distribution, and possibly the transport of material within the particle by diffusion or viscous flow. In aerosol formation processes, ambient pressures are normally near one atmosphere. However, the pressure within the particles may be much greater. The relationship between interior pressure and particle size is given by the Laplace-Young equation,

$$P_i - P_a = 2\sigma/r \quad (9)$$

where P_i is the particle interior pressure, P_a is the ambient pressure, σ is the surface tension, and r is the particle radius. In the derivation of this equation, the surface tension is assumed to be constant with respect to particle size (Landau and Lifshitz, 1958). This assumption may break down for very small particles. However, recent molecular dynamics calculations of the properties of silicon clusters at high temperatures reveal that material properties such as surface tension and diffusivity approach bulk values for clusters as small as 30 atoms (Zachariah *et al.*, 1996). As an example of how high the pressure may be inside these nanometer sized particles, the pressure inside a 10 nm diameter TiO_2 particle ($\sigma \sim 0.5 \text{ J m}^{-2}$; Bruce, (1965)) is on the order of 2000 atmospheres.

CONCLUSIONS

Single component silica and titania aerosols were formed in a laminar premixed flat flame from SiBr_4 , SiCl_4 , HMDS and TiCl_4 . The average silica primary particle diameter was 10 nm. The titania particles were slightly larger than the silica particles, average diameter of 13 nm. Predictions of primary particle size were made using the collision/sintering theory of

Koch and Friedlander (1990). The observed primary particle size of the titania aerosol compared well with predictions of primary particle size when a characteristic coalescence time derived from literature values for the solid state diffusion coefficient was used. The final primary particle size of silica was underpredicted for the two coalescence times used in the model.

Mixed SiO₂/TiO₂ aerosols, average diameter = 15 nm, were formed from three sets of precursors, SiBr₄/TiCl₄, SiCl₄/TiCl₄, and HMDS/TiCl₄. Single particle chemical analysis of the mixed particles using EDS showed only slight variations in composition from particle to particle, with no pure particles of either species detected. The choice of silica precursor had no observed effect on the distribution of species from particle to particle. In a premixed flame environment, the high concentrations of radical species imply that the precursor oxidation chemistry will be dominated by reactions involving radicals, and therefore will be very fast relative to the particle formation processes. Application of a simple criteria, developed for runaway nucleation in single component systems by Zachariah and Dimitriou (1990), to the general case of binary particle formation confirmed that differences in precursor chemistry may affect interparticle homogeneity for systems in which thermal decomposition reactions govern precursor decomposition. However, for radical driven chemistries, particle growth is independent of precursor species.

Use of EELS to probe the distribution of species on a nanometer scale revealed areas of chemical segregation within the particles, an expected result considering the equilibrium phase distribution of the SiO₂/TiO₂ system at the maximum flame temperature of the system. It is interesting that this phenomenon is occurring on the nanometer scales of the materials formed in these experiments.

Acknowledgements—This work was supported by the National Science Foundation, grant CTS 92-18222, and by the Los Alamos Cooperative Research Program, grant 6860V0016. The authors also acknowledge Dr. Dale Newbury and Dr. Richard Leapman for performing the EELS analysis.

REFERENCES

- Akhtar, M. K., Pratsinis, S. E. and Mastrangelo, S. V. R. (1992) Dopants in vapor-phase synthesis of titania powders. *J. Am. Ceram. Soc.* **75**, 3408.
- Akhtar, M. K., Pratsinis, S. E. and Mastrangelo, S. V. R. (1994) Vapor phase synthesis of Al-doped titania powders. *J. Mater. Res.* **9**, 1231.
- Akhtar, M. K., Xiong, Y. and Pratsinis, S. E. (1991) Vapor synthesis of titania powder by titanium tetrachloride oxidation. *A.I.Ch.E. J.* **37**, 1561.
- Anderson, H. U. (1967) Initial sintering of rutile. *J. Am. Ceram. Soc.* **50**, 235.
- Astier, M. and Vergnon, P. (1976) Determination of the diffusion coefficients from sintering data of ultrafine oxide particles. *J. Solid State Chem.* **19**, 67.
- Backer, M. R., Cavender, R., Elder, M. L., Jones, P. C. and Murphy, J. A. (1991) Method of manufacturing optical waveguide fiber with titania-silica outer cladding. U.S. Patent Number 5,067, 975.
- Bradley, D. and Matthews, K. J. (1968) Measurement of high gas temperatures with fine wire thermocouples. *J. Mech. Engng. Sci.* **10**, 299.
- Bruce, R. H. (1965). In *Science of Ceramics*, Vol. 2 (Edited by Steward, G. H.), pp. 359–367. Academic Press, New York.
- Chung, S.-L. and Katz, J. L. (1985) The counterflow diffusion flame burner: a new tool for the study of the nucleation of refractory compounds. *Combust. Flame.* **61**, 271.
- DeVries, R. C., Roy, R. and Osborn, E. F. (1954) The System TiO₂-SiO₂. *Trans. Br. Ceram. Soc.* **53**, 525.
- Eberhart, J. P. (1991) *Structural and Chemical Analysis of Materials*. Wiley, New York.
- Ehrman, S. E. (1997) Formation of binary oxide aerosols in premixed flames: factors influencing the segregation of species. Ph.D. thesis. University of California, Los Angeles.
- Formenti, M., Juillet, F., Meriaudeau, P., Teichner, S. J. and Vergnon, P. (1972) Preparation in a hydrogen-oxygen flame of ultrafine metal oxide particles. Oxidative properties toward hydrocarbons in the presence of ultraviolet radiation. In *Aerosols and Atmospheric Chemistry* (Edited by Hidy, G. M.). Academic Press, New York.
- French, W. G., Pace, L. J. and Foertmeyer, V. A. (1978) Chemical kinetics of the reactions of SiCl₄, SiBr₄, GeCl₄, POCl₃ and BCl₃ with oxygen. *J. Phys. Chem.* **82**, 2191.
- Frenkel, J. (1945) Viscous flow of crystalline bodies under the action of surface tension. *J. Phys.* **9**, 385.
- Friedlander, S. K. and Wu, M. K. (1994) Linear rate law for the decay of the excess surface area of a coalescing solid particle. *Phys. Rev. B.* **49**, 3622.
- Fristrom, R. M. (1995) *Flame Structure and Processes*. Oxford University Press, New York.
- Glassman, I. (1977) *Combustion*. Academic Press, New York.
- Greegor, R. B., Lytle, F. W., Sandstrom, D. R., Wong, J. and Schultz, P. (1983) Investigation of TiO₂-SiO₂ glasses by X-ray absorption spectroscopy. *J. Non-Crystalline Solids.* **55**, 27.

- Hering, S. V., Friedlander, S. K., Collins, J. J. and Richards, L. W. (1979) Design and evaluation of a new low-pressure impactor. 2. *Environ. Sci. Technol.* **13**, 184.
- Hetherington, G., Jack, K. H. and Kennedy, J. C. (1964) The viscosity of vitreous silica. *Phys. Chem. Glasses* **5**, 130.
- Hinds, W. C. (1982) *Aerosol Technology*. Wiley-Interscience, New York.
- Hren, J. J., Goldstein, J. I. and Joy, D. C. (1979) *Introduction to Analytical Electron Microscopy*. Plenum Press, New York.
- Hung, C.-H. and Katz, J. L. (1992) Formation of mixed oxide powders in flames: part 1. TiO_2 - SiO_2 . *J. Mat. Res.* **7**, 1861.
- Hung, C.-H., Miquel, P. F. and Katz, J. L. (1992) Formation of mixed oxide powders in flames: part 2., GeO_2 - SiO_2 , and Al_2O_3 - TiO_2 . *J. Mat. Res.* **7**, 1870.
- Kato, A., Kawazoe, S. and Mochida, I. (1972) Preparation of finely-divided alumina by vapor phase reaction between aluminum chloride and oxidizing gases, and its properties. *Zairyo* **21**, 540.
- Ko, E. I., Chen, J.-P. and Weissman, J. G. (1987) A study of acidic titania/silica mixed oxides and their use as supports for nickel catalysts. *J. Catal.* **105**, 511.
- Kobata, A., Kusakabe, K. and Morooka, S. (1991) Growth and transformation of TiO_2 crystallites in an aerosol reactor. *A.I.Ch.E. J.* **37**, 347.
- Koch, W. and Friedlander, S. K. (1990) The effect of particle coalescence and agglomeration on the surface area of a coagulating aerosol. *J. Colloid Interface Sci.* **140**, 419.
- Kumbhar, P. S. (1993) Nickel supported on titania-silica: preparation, characterization and activity for liquid-phase hydrogenation of acetophenone. *Appl. Catal. A.* **96**, 241.
- Landau, L. D. and Lifshitz, E. M. (1958) *Statistical Physics*. Pergamon, London.
- Lehtinen, K. E. J., Windeler, R. S. and Friedlander, S. K. (1996) A note on the growth of primary particles in agglomerate structures by coalescence. *J. Colloid Interface Sci.* **182**, 606.
- Liu, Z. and Davis, R. J. (1994) Investigation of the structure of microporous Ti-Si mixed oxides by X-ray, UV reflectance, FT-Raman, and FT-IR spectroscopies. *J. Phys. Chem.* **98**, 1253.
- MacKenzie, K. J. D. (1975) The calcination of titania: IV. The effect of additives on the anatase-rutile transformation. *Trans. Br. Ceram. Soc.* **74**, 29.
- Miquel, P. F., Hung, C.-H. and Katz, J. L. (1993) Formation of V_2O_5 -based mixed oxides in flames. *J. Mat. Res.* **8**, 2404.
- Peppiatt, S. J. (1975) The melting of small particles. II. Bismuth. *Proc. Roy. Soc. London A.* **345**, 401.
- Parikh, N. M. (1958) Effect of atmosphere on surface tension of glass. *J. Am. Ceram. Soc.* **41**, 18.
- Pratsinis, S. E., Bai, H., Biswas, P., Frenklach, M. and Mastrangelo, S. V. R. (1990) Kinetics of titanium (IV) chloride oxidation. *J. Am. Ceram. Soc.* **73**, 2158.
- Pratsinis, S. E. and Mastrangelo, S. V. R. (1989) Material synthesis in aerosol reactors. *Chem. Engng. Prog.* **85**, 62.
- Sanogo, O. and Zachariah, M. R. (1997) Kinetic studies of the reaction of tetraethoxysilane (TEOS) with oxygen atoms. *J. Electrochem. Soc.* **144**, 2919.
- Scholze, H. (1991) *Glass: Nature, Structure, and Properties*. Springer, New York.
- Schultz, P. C. (1976) Binary titania-silica glasses containing 10 to 20 wt% TiO_2 . *J. Am. Ceram. Soc.* **59**, 214.
- Shannon, R. D. and Pask, J. A. (1965) Kinetics of the anatase-rutile transformation. *J. Am. Ceram. Soc.* **48**, 391.
- Shannon, R. D. and Prewitt, C. T. (1969) Effective ionic radii in oxides and fluorides. *Acta Crystal.* **B25**, 925.
- Sohn, J. R. and Jang, H. J. (1991) Correlation between the infrared band frequency of the silanol bending vibration in TiO_2 - SiO_2 catalysts and activity. *J. Catal.* **132**, 563.
- Solomon, D. H. and Hawthorne, D. R. (1991) *Chemistry of Pigments and Fillers*. Wiley, New York.
- Ulrich, G. D. (1971) Theory of particle formation and growth in oxide synthesis flames. *Combust. Sci. Technol.* **4**, 47.
- Ulrich, G. D. (1984) Flame synthesis of fine particles. *Chem. Engng. News*. August 6.
- Vemury, S. and Pratsinis, S. E. (1995) Dopants in flame synthesis of titania. *J. Am. Ceram. Soc.* **78**, 2984.
- Westenberg, A. A. and DeHaas, N. (1975) Rates of $\text{H} + \text{CH}_3\text{X}$ reactions. *J. Chem. Phys.* **62**, 3321.
- Williams, D. B. and Carter, C. B. (1996) *Transmission Electron Microscopy IV, Spectrometry*. Plenum, New York.
- Windeler, R. S., Lehtinen, K. E. J. and Friedlander, S. K. (1997a) Production of nanometer sized metal oxide particles by gas phase reaction in a free jet I: experimental system and results. *Aerosol Sci. Technol.* **27**, 174.
- Windeler, R. S., Lehtinen, K. E. J. and Friedlander, S. K. (1997b) Production of nanometer sized metal oxide particles by gas phase reaction in a free jet II: particle size and neck formation—comparison with theory. *Aerosol Sci. Technol.* **27**, 191.
- Xiong, Y., Akhtar, M. K. and Pratsinis, S. E. (1993) Formation of agglomerate particles by coagulation and sintering. Part II. The evolution of the morphology of aerosol-made titania, silica, and silica-doped titania powders. *J. Aerosol Sci.* **24**, 301.
- Zachariah, M. R. (1990) Modeling ceramic sub-micron particle formation from the vapor using detailed chemical kinetics: comparison with in-situ laser diagnostics. *Chem. Engng. Sci.* **45**, 2551.
- Zachariah, M. R. (1997) Unpublished data for decomposition of HMDS, method following Sanogo and Zachariah (1997).
- Zachariah, M. R., Aquino, M. I., Shull, R. D. and Steel, E. B. (1995a) Formation of superparamagnetic nanocomposites from vapor phase condensation in a flame. *Nanostructured Mat.* **5**, 383.
- Zachariah, M. R., Carrier, M. J. and Blaisten-Barojas, E. (1996) Properties of silicon nanoparticles, a molecular dynamics study. *J. Phys. Chem.* **100**, 14856.
- Zachariah, M. R. and Dimitriou, P. (1990) Controlled nucleation in aerosol reactors for suppression of agglomerate formation: a numerical study. *Aerosol Sci. Technol.* **13**, 413.
- Zachariah, M. R. and Semerjian, H. G. (1990) Experimental and numerical studies on refractory particle formation in flames. *High Temp. Sci.* **28**, 113.
- Zachariah, M. R., Shull, R. D., McMillin, B. K. and Biswas, P. (1995b) *In situ* characterization and modeling of the vapor-phase formation of a magnetic nanocomposite. In *Nanotechnology: Molecularly Designed Materials* (Edited by Chow, G. M. and Gonsalves, K. E.). American Chemical Society, Washington, DC.
- Zachariah, M. R. and Tsang, W. (1993) Application of *ab initio* molecular orbital and reaction rate theories to nucleation kinetics. *Aerosol Sci. Technol.* **19**, 499.